

Dehydrogenation of Formic Acid Catalyzed by a Ruthenium Complex with an *N,N'*-Diimine Ligand

Chao Guan,<sup>†,⊥</sup> Dan-Dan Zhang,<sup>†,⊥</sup> Yupeng Pan,<sup>†</sup> Masayuki Iguchi,<sup>‡</sup> Manjaly J. Ajitha,<sup>†</sup> Jinsong Hu,<sup>†</sup> Huaifeng Li,<sup>†</sup> Changguang Yao,<sup>†</sup> Mei-Hui Huang,<sup>†</sup> Shixiong Min,<sup>†</sup> Junrong Zheng,<sup>§</sup> Yuichiro Himeda,<sup>||</sup> Hajime Kawanami,<sup>‡</sup> and Kuo-Wei Huang<sup>\*,†,⊥</sup>

<sup>†</sup>KAUST Catalysis Center and Division of Physical Sciences and Engineering, King Abdullah University of Science and Technology, Thuwal 23955-6900, Saudi Arabia

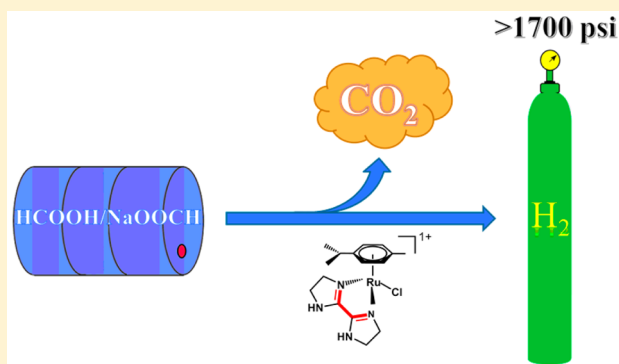
<sup>‡</sup>National Institute of Advanced Industrial Science and Technology, 4-2-1 Nigatake, Miyagino-ku, Sendai, Miyagi 983-8551, Japan

<sup>§</sup>College of Chemistry, Peking University, Beijing 100871, China

<sup>||</sup>National Institute of Advanced Industrial Science and Technology, 1-1-1 Higashi, Tsukuba-shi, Ibaraki 305-8565, Japan

**S** Supporting Information

**ABSTRACT:** We report a ruthenium complex containing an *N,N'*-diimine ligand for the selective decomposition of formic acid to H<sub>2</sub> and CO<sub>2</sub> in water in the absence of any organic additives. A turnover frequency of 12 000 h<sup>-1</sup> and a turnover number of 350 000 at 90 °C were achieved in the HCOOH/HCOONa aqueous solution. Efficient production of high-pressure H<sub>2</sub> and CO<sub>2</sub> (24.0 MPa (3480 psi)) was achieved through the decomposition of formic acid with no formation of CO. Mechanistic studies by NMR and DFT calculations indicate that there may be two competitive pathways for the key hydride transfer rate-determining step in the catalytic process.



## INTRODUCTION

Formic acid (FA) has recently been proposed as a chemical hydrogen (H<sub>2</sub>) carrier because of its favorable properties.<sup>1</sup> FA contains 4.4 wt % of hydrogen, and it is liquid under ambient conditions, allowing it to be handled, stored, and transported easily and safely. Although the decomposition of FA to H<sub>2</sub> and carbon dioxide (CO<sub>2</sub>) was discovered half a century ago by Coffey using an iridium (Ir) phosphine complex with a high turnover frequency (TOF) (1187 h<sup>-1</sup>) and a high turnover number (TON) (>11 000),<sup>2</sup> this reaction has been investigated extensively only in the past decade. Several transition metal complexes based on iron,<sup>3</sup> rhodium,<sup>4</sup> ruthenium,<sup>5</sup> and iridium<sup>6</sup> have been demonstrated as active catalysts for the dehydrogenation of FA. From these systems, those with high TON in aqueous solution are of particular interest. For example, Himeda, Fujita, and co-workers reported an iridium-bipyridine catalyst with a TON of 308 000 h<sup>-1</sup>.<sup>6j</sup> Most impressively, Li and co-workers later demonstrated that by using *N,N'*-diimine ligands, the resulting Ir complexes showed unprecedentedly high reactivities for the dehydrogenation of FA with a remarkable TON of 2 400 000.<sup>6c</sup> While these systems offer a great potential for practical applications, the high price of Ir prompts us to explore a more economic option. As ruthenium (Ru) complexes typically have very similar properties to Ir analogues, we were inspired to investigate the activity

and feasibility of Ru catalysts with an *N,N'*-diimine ligand for the decomposition of FA. Herein, we report the reactivity and mechanistic studies of the dehydrogenation of FA using a newly developed Ru compound with 2,2'-biimidazoline.

## RESULTS AND DISCUSSION

**Formic Acid Decomposition.** Complex **1** was prepared at room temperature from the precursor [Ru(*p*-cymene)Cl<sub>2</sub>]<sub>2</sub> and ligand (2,2'-biimidazoline) (Scheme 1). A suitable single crystal (Figure 1) was obtained from a solution of complex **1** in the mixed solvent of ether and DMSO for X-ray crystallography. A *p*-cymene ( $\eta^6$ ) is coordinated to the Ru center with a chloride and 2,2'-biimidazoline ligands to give a saturated 18-electron cationic complex. Complex **1** is intrinsically stable in air and is water-soluble (30 mg/mL).

The decomposition of FA was examined with various FA/HCOONa ratios in an aqueous solution at 90 °C (Table 1). Using FA solution, an initial TOF of 3750 h<sup>-1</sup> (Table 1, entry 1) was obtained, and this rate of decomposition doubled when one equivalent of HCOONa (SF) was mixed in the FA solution (8150 h<sup>-1</sup>) (Table 1, entry 2). No obvious change in TOF was identified when Na<sub>2</sub>SO<sub>4</sub> was added, indicating that the observed

Received: September 28, 2016

Published: December 16, 2016

## Scheme 1. Preparation of Complex 1

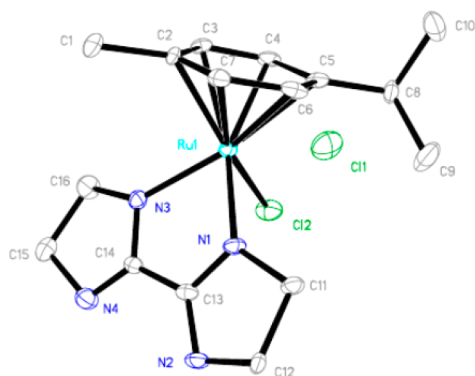
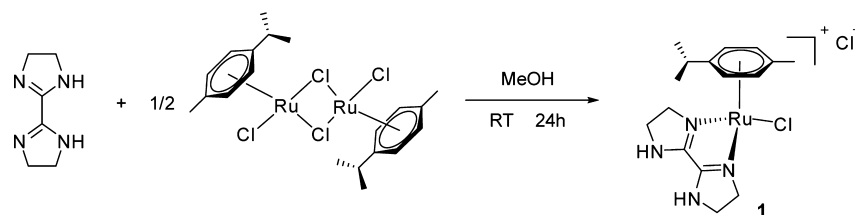


**Figure 1.** Molecular structure of complex **1** with thermal ellipsoids set at 40% probability. Hydrogen atoms were omitted for clarity. Selected bond lengths (Å): Ru1–N3 2.086(4), Ru1–N1 2.087(3), Ru1–C2 2.175(4), Ru1–C3 2.161(4), Ru(1)–C(4) 2.202(4), Ru(1)–C(5) 2.180(4), Ru(1)–C(6) 2.179(4), Ru(1)–C(7) 2.206(4), and Ru1–Cl2 2.4021(11); selected bond angles (deg): N1–Ru1–N3 75.76(14).

**Table 1.** Dehydrogenation of FA/SF in Water Using Complex **1**<sup>a</sup>

entry	SF/FA	FA (10 <sup>-2</sup> mol)	cat. (10 <sup>-2</sup> mol %)	TOF <sub>max</sub> (h <sup>-1</sup> )	TON	yield (%)
1	0	2.5	0.8	3750	11 670	93
2	1	2.5	0.8	8150	10 100	80
3	2	2.5	0.8	9400	10 420	83
4	5	1	2	12 000	4170	83
5	10	0.5	4	8250	2300	91

<sup>a</sup>General: No reaction occurred in the absence of catalysts. Each reaction was repeated at least twice with an error of less than 5%. The maximum TOF was estimated based on the H<sub>2</sub> production in the first 10 min. TONs and yields were determined when the reaction stopped and no more gas was generated. Temperature: 90 °C. All the initial volumes of reaction solutions are 5.0 mL.

acceleration of the reaction was not due to the presence of Lewis acidic Na<sup>+</sup> (Table S1).<sup>3b</sup> A maximum TOF of 12 000 h<sup>-1</sup> (Table 1, entry 4) was achieved when the ratio of SF/FA was increased to 5. Little gas formation was observed when heating the aqueous SF solution (5.0 M) in the presence of complex **1** at 90 °C, suggesting that formate cannot be decomposed directly in this Ru system.<sup>7</sup> In all cases, the composition of the evolved gas was confirmed to be an equimolar mixture of H<sub>2</sub> and CO<sub>2</sub> with no trace amount of CO detected (Figure S1). These observations indicate that the decomposition of FA catalyzed by complex **1** is highly selective and produces only H<sub>2</sub> and CO<sub>2</sub>, making this system suitable for application to fuel cells, in which CO poisoning of electrodes must be prevented.<sup>8</sup>

## MECHANISM STUDIES

**Activation Energy.** The activation energy ( $E_a$ ) was obtained by measuring the initial rates from 60 to 90 °C

in a 1:1 mixture of FA/SF solution. The estimated apparent activation energy by the Arrhenius plot is  $23 \pm 0.5$  kcal/mol (Figure 2), within the range of those of FA dehydrogenation reactions catalyzed by noble metals.<sup>3d</sup>

**Plausible Active Species.** Mass spectrometry was employed to identify plausible active species in the absence or presence of HCOONa in water. In the absence of HCOO<sup>-</sup>, mass peaks were observed at  $m/z = 409$ , 187, and 373 and were assigned to **IN1**, **A**, and **IN5**, respectively (Scheme 2). A chloride can be dissociated from **IN1** ( $m/z = 409$ ) to form **A** ( $m/z = 187$ ) in the aqueous solution. **A**, a binary weak acid, may go through a deprotonation to give **IN5** ( $m/z = 373$ ). When HCOONa was added (Figure S3), the same mass peaks were obtained, but the intensity of the 373 peak increased, suggesting that the presence of more HCOO<sup>-</sup> species led to the formation of more **IN5** species. Although **IN5** may be further deprotonated to afford a neutral complex (**B**), **B** could not be monitored by mass spectrometry. Because the equilibria between these species are pH-sensitive, a pH-dependence study on the initial TOFs was conducted. The results showed that the highest TOF was achieved at pH = 4.3, where the concentration of species **IN5** was the highest, suggesting that **IN5** may play an important role in the catalytic process.

Next, we employed NMR to gain additional structural insights. Two new peaks were found in the solution of complex **1** in 1:5 of H<sub>2</sub>O and D<sub>2</sub>O compared to those of complex **1** in D<sub>2</sub>O alone (Figure S4). Note that these two peaks disappeared when the temperature was increased to 50 °C and reappeared when cooled to 25 °C. The intensity of these peaks increased with the increasing ratio of H<sub>2</sub>O/D<sub>2</sub>O (5:1). On the basis of these observations, we rationalized that these two peaks belong to a water ligand (**IN2**) that can exchange with the chloride.

When HCOONa (50 μmol) was added to a D<sub>2</sub>O solution of complex **1** (10 μmol in 0.5 mL of D<sub>2</sub>O) at 90 °C for 2 min (Figure S5), no obvious reaction was observed and HCOO<sup>-</sup> did not completely decompose. Two hydride signals ( $\delta -6.70$  and  $-7.70$  ppm) were observed, indicating the presence of two Ru–H species. When HCOOH (10 μL) and H<sub>2</sub>O (0.1 mL) were then added (Figure S6), within 2 min at 90 °C, the HCOOH signal had almost completely disappeared. Because the ruthenium hydride signal was not observed under acidic reaction conditions, we inferred that the reaction between the hydride complex and FA (or H<sub>3</sub>O<sup>+</sup>) to produce H<sub>2</sub> is fast, consistent with the regeneration of **IN2**.

On the basis of these observations, we proposed a plausible reaction mechanism, comprising two different pathways depending on the reaction conditions (Scheme 3). In the reaction involving only an aqueous FA solution, the water-coordinated ruthenium complex **IN2** is generated and the water ligand can be replaced by a formate to give complex **IN3**. Hydride complex **IN4** is formed after the decarboxylation of formate **IN3**. The aqua ruthenium complex **IN2** can be regenerated with the production of H<sub>2</sub> in the presence

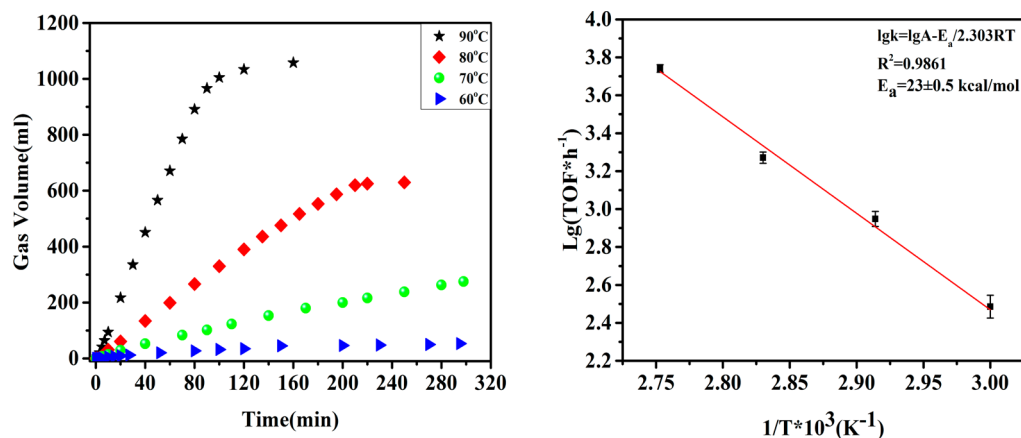


**Figure 2.** (a) Relationship between volume of gases and time to decompose FA using complex **1** ( $0.8 \times 10^{-2}$  mol %) (FA (5 mL 5[M]), [FA]:[SF] = 1:1;  $T = 90, 80, 70, 60$  °C). (b) Arrhenius plot of initial TOF values (first 10 min) for decomposition of FA using complex **1** (FA (5 mL 5[M]), [FA]:[SF] = 1:1).

### Scheme 2. Different Species from the Aqueous Solution of Complex 1 Observed under ESI

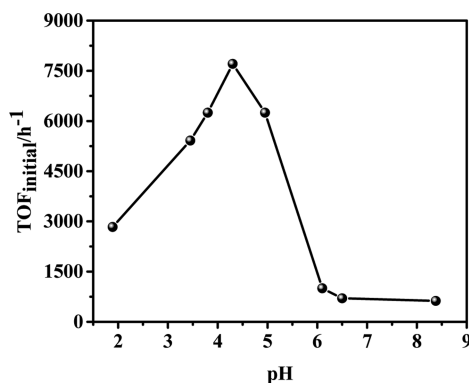
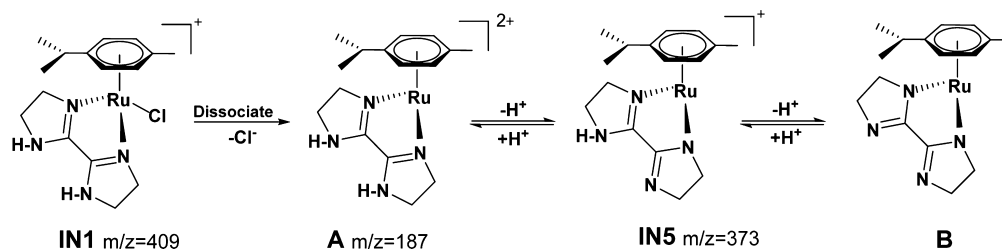


**Figure 3.** PH dependence of the initial TOF on decomposition of FA. Conditions: Complex **1** (2.0  $\mu\text{mol}$ ); FA/SF (1.0 [M], 10 mL);  $T = 90$  °C. The initial pH values were regulated by changing the ratio of NaOOCH and HCOOH.

of  $\text{H}_3\text{O}^+$ . Under slightly more basic conditions, in the presence of formate, IN1 may be deprotonated with the loss of a chloride to give intermediate IN5 (Scheme 2). Coordination of formate to IN5 generates complex IN6, which may be in equilibrium with IN3 and may undergo decarboxylation to give IN7.

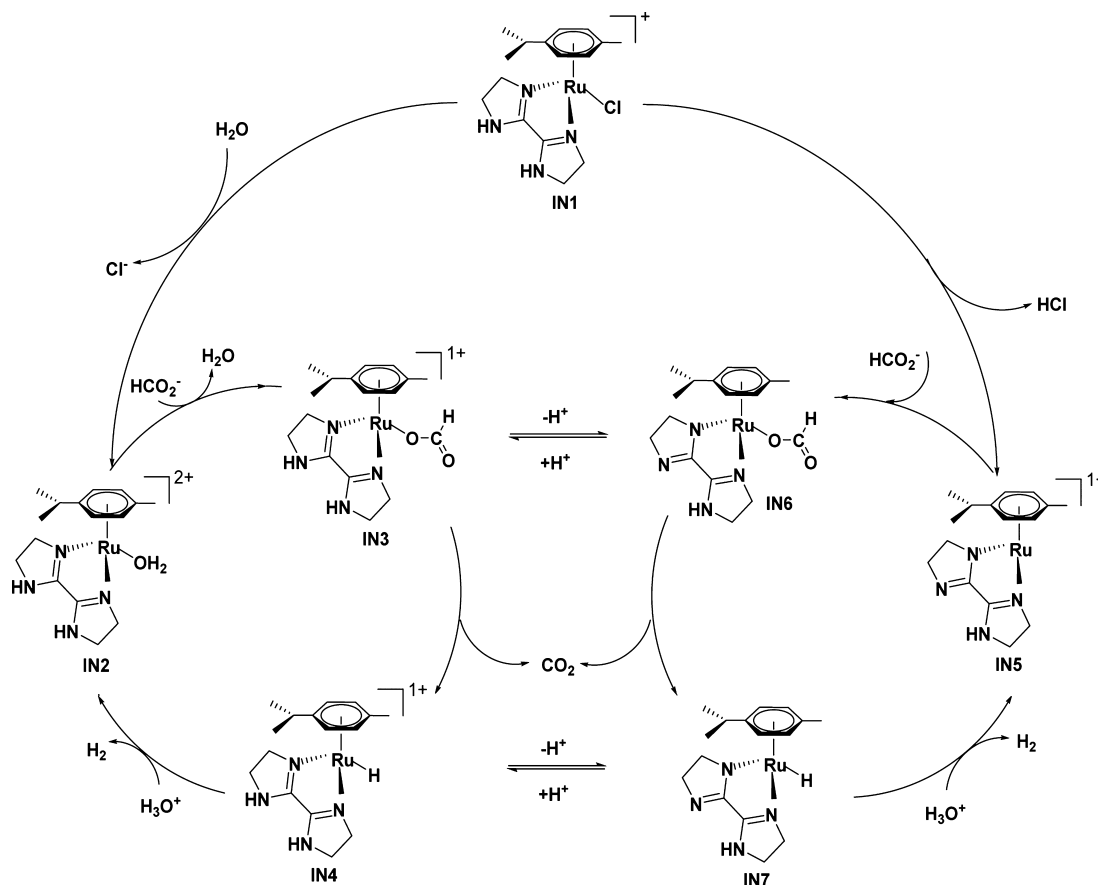
**Kinetic Isotope Effect (KIE).** KIE experiments were conducted to identify the rate-determining step (RDS) in the catalytic process. As shown in Table 2, the KIE value was  $2.1 \pm 0.3$  when  $\text{DCO}_2\text{H}$  was used (entry 2) and  $1.4 \pm 0.2$  when  $\text{HCO}_2\text{D}$  was employed (entry 3). Note that a maximum KIE of  $3.3 \pm 0.4$  was obtained with  $\text{DCO}_2\text{D}$  in  $\text{D}_2\text{O}$  (entry 4). These observations suggest that the decarboxylation involving the formyl C–H bond cleavage was most likely the RDS in the catalytic cycle.

**Optimized Catalytic Performance.** The performance of our catalytic system was further optimized by adding formic acid at a constant rate, as determined such that the rates of consumption and addition of FA were the same; a maximum TON of 350 000 was achieved in approximately 35 h (Figure 4).

**High-Pressure Gas Evolution.** We further evaluated the performance of the catalyst in terms of the production of high-pressure gases. The experimental procedure and the apparatus used have been described in previous reports.<sup>9</sup> Figure 5 shows the time course of the high-pressure evolution of gas from FA in the presence of catalyst **1**. Using 6.5 M formic acid free from sodium formate, high-pressure gases (24.0 MPa) ( $\text{CO}_2:\text{H}_2 = 1:1$ ) with 1.8 MPa of He (total 25.8 MPa) were obtained within 4 h. No CO was detected from the analysis of the gas mixture using GC/TCD at a minimum detection limit of 6 ppm. The final conversion of formic acid was up to 98%. However, the TOF was lower than that under atmospheric pressure ( $3750 \text{ h}^{-1}$ , entry 1, Table 1) because of the resultant equilibrium between FA and  $\text{H}_2$  with  $\text{CO}_2$ .<sup>10</sup> Because the biimine ligand can effectively activate the Ru complex even under high-pressure conditions,<sup>11</sup> these results indicate that complex **1** could be a possible cost-effective catalyst for the hydrogen station to generate high-pressure hydrogen gas instead of analogous Ir complexes.

**Computational Mechanism Studies.** Calculations were carried out to assess the proposed mechanism in Scheme 3 and to determine transition states and energy barriers for the reactions that were observed experimentally. The calculated free-energy profile shows the chloride ion IN1 is easily formed from the dimer complex  $[\text{RuCl}_2(p\text{-cymene})]_2$  (Figure S7). The optimized structure of the chloride complex IN1 is in good agreement with the X-ray structure.

Scheme 3. Proposed Mechanism for the Dehydrogenation of Formic Acid

Table 2. KIE in the Dehydrogenation for FA Using Complex 1<sup>a</sup>

entry	substrate	solvent	TOF <sup>b</sup> (h <sup>-1</sup> )	KIE
1	HCOOH	H <sub>2</sub> O	2550	
2	DCOOH	H <sub>2</sub> O	1200	2.1 ± 0.3
3	HCOOD	D <sub>2</sub> O	1800	1.4 ± 0.2
4	DCOOD	D <sub>2</sub> O	800	3.1 ± 0.4

<sup>a</sup>Reaction conditions: Complex Ru (2.0 μmol), FA solution (2.5 M, 5.0 mL), 90 °C. <sup>b</sup>TOF was calculated for the first 10 min.

The detailed free-energy profile for the proposed mechanism in Scheme 3 is shown in Figure 6, and the corresponding structural parameters are presented in Figure 7. For the hydride transfer from the chloride complex IN1 to the hydride complex IN4, two possible pathways were evaluated (green and blue paths in Figure 6).

In the green pathway, the replacement of the chloride ligand in IN1 by water gives intermediate IN2, which is endothermic by 7.8 kcal/mol. The coordination of a formate anion at the Ru center is favorable with a bond length of 2.101 Å to give the more stable formate intermediate IN3 with -1.0 kcal/mol, relatively superior to the intermediate IN1. The outer-sphere hydride transfer-transition state TS1 was located, where the Ru-H bond and C-H bonds were 2.246 and 1.172 Å, respectively. The active barrier from IN3 to TS1 was 21.3 kcal/mol. The inner-sphere β-H elimination transition state S-TS1 involving the breakage of the Ru-N coordination bond was also located (Figure S8), but the corresponding active barrier was higher than that of TS1 (25.5 kcal/mol vs 21.3 kcal/mol).

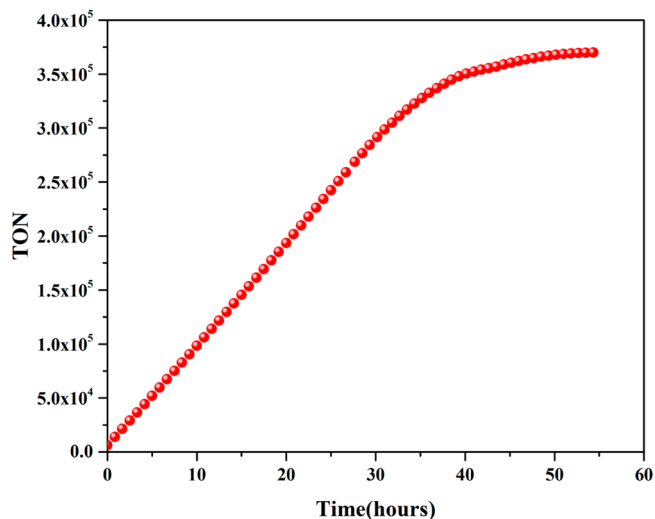
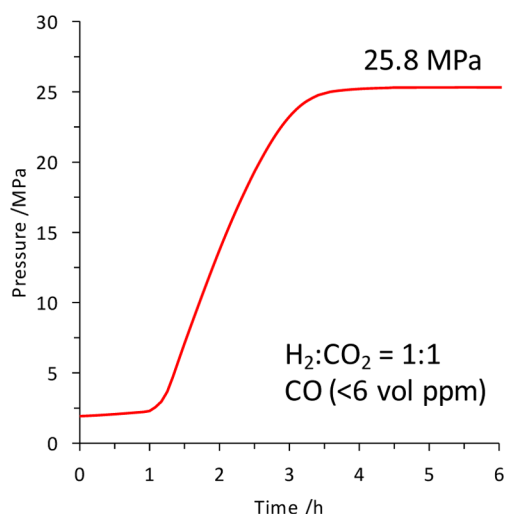


Figure 4. Optimized performance of complex 1. Reaction conditions: Ru (0.50 μmol), 90 °C, FA (2.0 M, 10.0 mL), [FA]:[SF] = 1:5; FA was added to the FA/SF solution at 0.2 mL/h.

The release of CO<sub>2</sub> gives the key proposed hydride intermediate IN4 at -1.9 kcal/mol, relatively superior to IN1.

In the blue pathway, transition state TS2 describes the deprotonation of one of the NH moieties by a formate anion with a low active barrier of 6.8 kcal/mol. Note that the following intermediate IN5 losing the chloride ligand and the proton of the NH group is in good agreement with our experimental observations. Formate intermediate IN6 has



**Figure 5.** Time-dependent gas evolution through FA decomposition in the presence of catalyst **1**. The reaction was carried out at 80 °C in an autoclave (internal volume is 7.0 mL) with 2 MPa of He gas, FA aqueous solution (6.5 mol/L, 4.0 mL), and catalyst (8.0 mol, 2.0 mmol/L).

shorter Ru–N bonds with a higher free energy compared to **IN3**. However, the outer-sphere hydride transfer transition state **TS3** has a free energy similar to that of **TS1** (20.2 vs 20.3 kcal/mol). From the structural parameters, **TS3** is characterized as an early transition state with a Ru–H bond of 2.523 Å and a C–H bond of 1.155 Å. After decarboxylation, intermediate **IN7** can also be readily protonated to give hydride intermediate **IN4**. On the basis of the comparable activation barriers and experimental observations, it seems likely that both blue and green pathways are competitive under our reaction conditions and that the blue pathway may be favorable under slightly more basic conditions.

For the protonation of hydride intermediate **IN4**, two proton sources, namely, formic acid and the hydrated proton, were investigated.<sup>12</sup> Transition state **TS4** with formic acid as the proton source has an activation energy barrier of 24.8 kcal/mol, 13.7 kcal/mol higher than that of transition state **TS5** with the hydrated proton (Figure 7). Note that transition state **TS4** could only be located by the intramolecular hydrogen bonds between the carbonyl oxygen of FA and the N–H group of the ligand and the transition state **TS5** could only be located by the N atom of

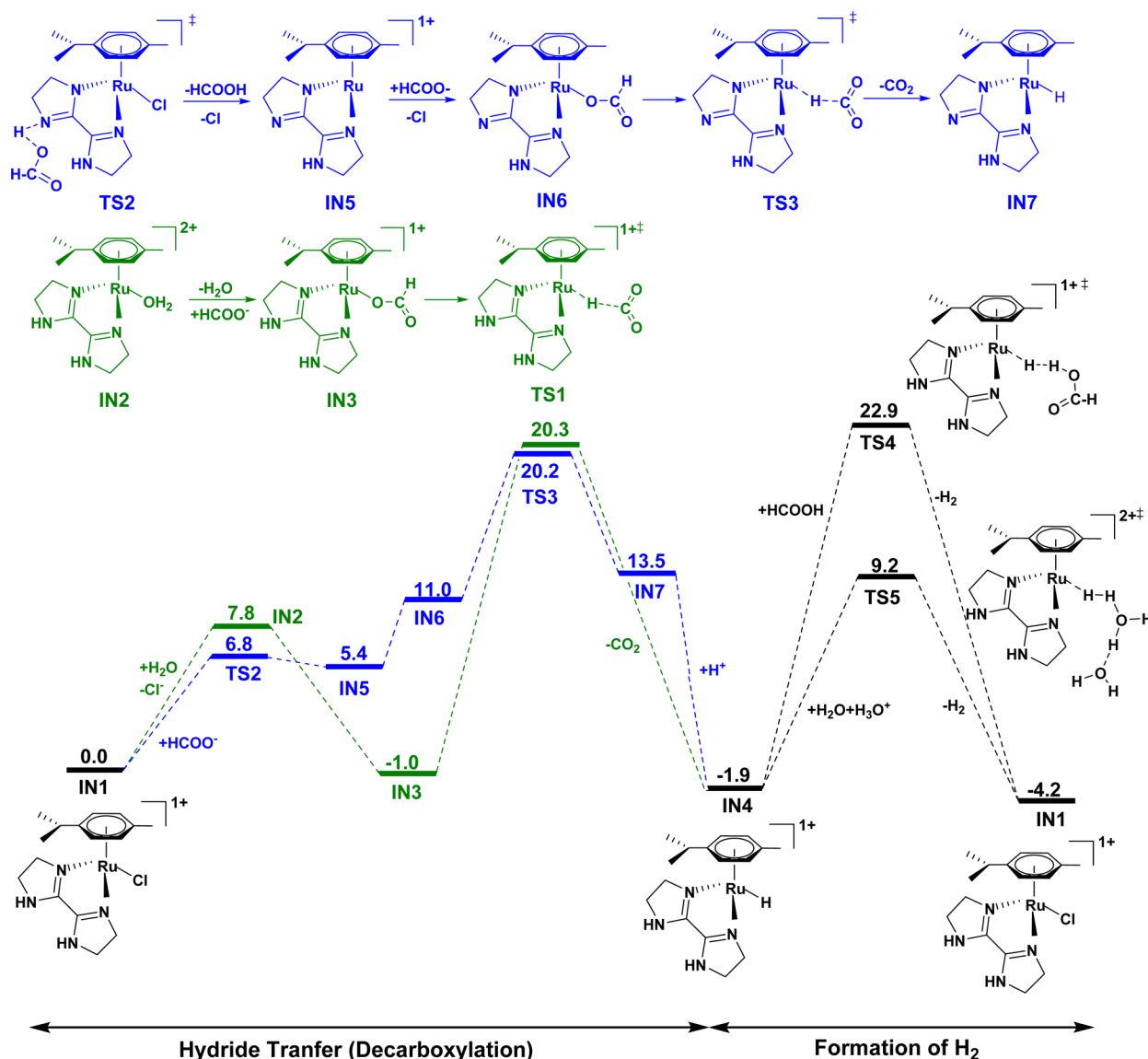


**Figure 6.** Relative free-energy profiles for the proposed mechanism in Scheme 3.

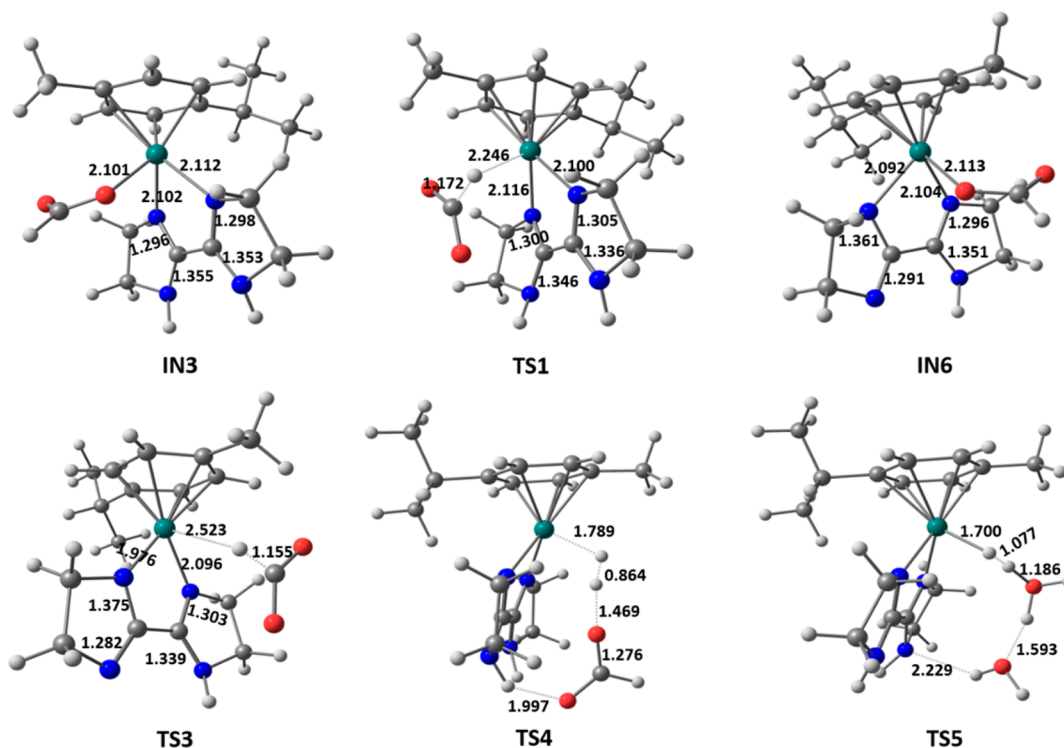


**Figure 7.** Optimized geometries of the hydride transfer transition states (TS1 and TS3) and intermediates (IN3 and IN6) as well as optimized geometries of the formation of H<sub>2</sub> transition states (TS4 and TS5). Atoms Ru, C, N, and O are shown in green, gray, blue, and red, respectively. Calculated bond distances are shown in Å.

the ligand and the O–H group of the bridging water. TS4 is considered more strained, as it possesses longer Ru–H (1.789 Å) and O–H bonds (1.469 Å) than those of TS5 (Ru–H, 1.700 Å; O–H, 1.186). Overall, the outer-sphere hydride transfer stage was the rate-determining step and shall proceed via comparable blue and green pathways. The computed KIE for the RDS was 2.0, in agreement with our experimental observations. The formation of H<sub>2</sub> then occurs via TS5 with a hydrated proton as the proton source.

## CONCLUSION

In summary, Ru complex **1** shows a good activity to give reasonably high TOF and TON of 12 000 h<sup>-1</sup> and 350 000, respectively. The first application of a ruthenium complex for the high-pressure hydrogen production from formic acid was realized. Experimental and density function theory studies were conducted to elucidate the plausible mechanism of the decomposition of FA/SF. Two competitive pathways were proposed for the key hydride transfer step. Further development using this catalyst system for hydrogen fuel cell applications is ongoing and will be reported in due course.

## EXPERIMENTAL SECTION

**General Procedures.** All experiments (if not mentioned otherwise) with metal complexes were carried out under an atmosphere of dry argon in a glovebox or using standard Schlenk techniques. All other chemicals were commercially available and used as received. <sup>1</sup>H and <sup>13</sup>C NMR spectra were recorded on a Bruker 400 or 600 MHz spectrometer at 400 and 100 MHz or 600 and 125 MHz for proton and carbon, respectively. Column chromatography was performed on silica gel (200–300 mesh). Results of the GC analysis were obtained with Techcomp GC7890II equipped with a TCD and a FID. The pH values were measured on a ZDJ-400DH multifunction titrator with a glass electrode after calibration to standard buffer

solutions. HRMS data were recorded on a Finnigan MAT 95 system. Elemental analyses were carried out on a Flash 2000 elemental analyzer. The X-ray diffraction data were collected using a Bruker-AXS KAPPA-APEXII CCD diffractometer. The N,N'-diimine ligand was synthesized,<sup>13</sup> and TON and TOF were calculated according to literature procedures.<sup>6e</sup>

**Synthesis and Characterization of Complex 1 [Ru(*p*-Cymene)(2,2'-biimidazole)Cl]Cl.** In a glovebox, dry methanol (30.0 mL) was added to a mixture of dichloro(*p*-cymene)ruthenium(II) dimer (0.20 mmol) and 2,2'-biimidazole (0.40 mmol) in a reaction flask and stirred overnight at room temperature. Methanol was then removed *in vacuo*. Column chromatography was used to purify the complex using CH<sub>2</sub>Cl<sub>2</sub>/MeOH (50:1–20:1) as the eluent. Yield: 60%. A single crystal of complex **1** was obtained from a mixture of DMSO and ether (1:20). <sup>1</sup>H NMR (600 MHz, DMSO-*d*<sub>6</sub>): δ 8.61 (s, 1H), 5.88 (d, *J* = 6.1 Hz, 2H), 5.60 (d, *J* = 6.0 Hz, 2H), 4.61–4.30 (m, 2H), 3.90–3.77 (m, 4H), 3.72 (dd, *J* = 24.6, 12.6 Hz, 2H), 2.71 (dt, *J* = 13.8, 6.9 Hz, 1H), 2.11 (s, 3H), 1.16 (d, *J* = 6.9 Hz, 6H). <sup>13</sup>C{<sup>1</sup>H} NMR (125 MHz, DMSO-*d*<sub>6</sub>): δ (ppm) 159.09, 102.37, 99.52, 83.08, 80.98, 55.39, 46.45, 31.15, 22.49, 18.97. MS *m/z* (ESI+) 409.1 [M – Cl]<sup>+</sup>. Anal. Calcd for C<sub>16</sub>H<sub>24</sub>Cl<sub>2</sub>RuN<sub>4</sub>: C 43.24, H 5.44, N 12.61. Found: C 42.79, H 5.63, N 12.73.

**General Procedure for Catalytic Dehydrogenation of HCO<sub>2</sub>H.** Decomposition of FA was performed in a two-necked round flask equipped with a reflux condenser and a magnetic stirrer at appropriate temperature. The aqueous catalyst stock solution was prepared freshly before use. The catalyst stock solution was injected through a septum into a flask with 5.0 mL of the FA (sodium formate) aqueous solution. The gas produced was monitored by an ADM 2000 flowmeter. The data were collected every 2 s. The water displacement method was used to confirm the amount of H<sub>2</sub> produced.

**Gas Composition Analysis.** The quantity of gas products during the decomposition of FA was measured using an online precalibrated gas chromatograph (Agilent 7890B) (H<sub>2</sub>, CO, CH<sub>4</sub>, CO<sub>2</sub>), and the identities of the gases were confirmed as H<sub>2</sub> and CO<sub>2</sub> with no detectable level of CO. The chromatograph was equipped with the following two channels: (1) two HayeSep Q columns and 13× molecular

sieves with a thermal conductivity detector using He as a carrier gas for CO<sub>2</sub> and CO analysis and (2) a HayeSep Q and 13X molecular sieves with a thermal conductivity detector using Ar as a carrier gas for H<sub>2</sub> analysis. After an initial reaction time of 1 min, the gas produced was analyzed by purging the produced gas directly to the online GC; the analysis began every 15 min. The molar ratio of H<sub>2</sub> and CO<sub>2</sub> was measured to be approximately 1:1 based on the calibration curve using a standard gas.<sup>5a</sup>

**Dehydrogenation of FA by Intermittent Addition of FA.** A stir bar and an FA/SF (2M, 1:5) aqueous solution were placed in a two-necked reaction flask. After the solution was preheated at 90 °C, the water solution of complex **1** (0.5 mL, 0.5 μmol) was injected into the flask. FA was added at a constant rate via a syringe pump based on the rate of consumption (0.1–0.3 mL/h).

**Computational Details.** All the calculations were performed in the Gaussian 09 program package.<sup>14</sup> The structures of all species were optimized with no geometry or symmetry constraints using the M06<sup>15</sup> functional with the BSI basis set (BSI denotes the basis set combination of SDD<sup>16</sup> for transition metals and the all-electron 6-31G(d,p) for N, O, H, and C). The M06 is a dispersion-corrected functional and can accurately estimate the reaction energy because of the consideration of weak interaction. The solvation effects of water solvent were considered by SMD<sup>17</sup> (solvation model density), a universal solvation model based on the polarized continuous quantum mechanical charge density of the solute. All stationary points were classified as minima or transition states by frequency calculations. Intrinsic reaction coordinate calculations at the same level of theory were carried out to confirm the right connections among a transition state and its forward and backward minima.<sup>18</sup> The energy of each species was refined by a single-point calculation at the M06/BSII-level coupled with an SMD solvent model (BSII denotes the basis set combination of SDD for Ru and the all-electron 6-311++G(2d,p) for N, O, H, C).

## ■ ASSOCIATED CONTENT

### Supporting Information

The Supporting Information is available free of charge on the ACS Publications website at DOI: 10.1021/acs.inorgchem.6b02334.

Additional supporting figures, tables, computational details, and Cartesian coordinates of the optimized geometries and energy parameters (PDF)  
Crystallographic data (CIF)

## ■ AUTHOR INFORMATION

### Corresponding Author

\*E-mail: hkw@kaust.edu.sa (K.-W. Huang).

### ORCID

Kuo-Wei Huang: 0000-0003-1900-2658

### Author Contributions

<sup>†</sup>C. Guan and D.-D. Zhang contributed equally to this work.

### Notes

The authors declare no competing financial interest.

## ■ ACKNOWLEDGMENTS

This work was supported by King Abdullah University of Science and Technology (KAUST). We thank Carolyn E. Unck for assistance with the manuscript preparation.

## ■ REFERENCES

(1) (a) Mellmann, D.; Sponholz, P.; Junge, H.; Beller, M. Formic acid as a hydrogen storage material - development of homogeneous catalysts for selective hydrogen release. *Chem. Soc. Rev.* **2016**, *45*, 3954–3988. (b) Wang, W.-H.; Himeda, Y.; Muckerman, J. T.; Manbeck, G. F.; Fujita, E. CO<sub>2</sub> Hydrogenation to Formate and

Methanol as an Alternative to Photo- and Electrochemical CO<sub>2</sub> Reduction. *Chem. Rev.* **2015**, *115*, 12936–12973. (c) Grasemann, M.; Laurenczy, G. Formic acid as a hydrogen source - recent developments and future trends. *Energy Environ. Sci.* **2012**, *5*, 8171–8181. (d) Fukuzumi, S.; Yamada, Y.; Suenobu, T.; Ohkubo, K.; Kotani, H. Catalytic mechanisms of hydrogen evolution with homogeneous and heterogeneous catalysts. *Energy Environ. Sci.* **2011**, *4*, 2754–2766. (e) Enthaler, S.; von Langermann, J.; Schmidt, T. Carbon dioxide and formic acid - the couple for environmental - friendly hydrogen storage? *Energy Environ. Sci.* **2010**, *3*, 1207–1217. (f) Johnson, T. C.; Morris, D. J.; Wills, M. Hydrogen generation from formic acid and alcohols using homogeneous catalysts. *Chem. Soc. Rev.* **2010**, *39*, 81–88. (g) Joó, F. Breakthroughs in Hydrogen Storage - Formic Acid as a Sustainable Storage Material for Hydrogen. *ChemSusChem* **2008**, *1*, 805–808. (h) Zaidman, B.; Wiener, H.; Sasson, Y. Formate salts as chemical carriers in hydrogen storage and transportation. *Int. J. Hydrogen Energy* **1986**, *11*, 341–347.

(2) Coffey, R. The Decomposition of Formic Acid Catalysed by Soluble Metal Complexes. *Chem. Commun. (London)* **1967**, 923–924.

(3) (a) Mellone, I.; Gorgas, N.; Bertini, F.; Peruzzini, M.; Kirchner, K.; Gonsalvi, L. Selective Formic Acid Dehydrogenation Catalyzed by Fe - PNP Pincer Complexes Based on the 2,6-Diaminopyridine Scaffold. *Organometallics* **2016**, *35*, 3344–3349. (b) Bielinski, E. A.; Lagaditis, P. O.; Zhang, Y.; Mercado, B. Q.; Würtele, C.; Bernskoetter, W. H.; Hazari, N.; Schneider, S. Lewis Acid-Assisted Formic Acid Dehydrogenation Using a Pincer - Supported Iron Catalyst. *J. Am. Chem. Soc.* **2014**, *136*, 10234–10237. (c) Zell, T.; Butschke, B.; Ben-David, Y.; Milstein, D. Efficient Hydrogen Liberation from Formic Acid Catalyzed by a Well - Defined Iron Pincer Complex under Mild Conditions. *Chem. - Eur. J.* **2013**, *19*, 8068–8072. (d) Boddien, A.; Mellmann, D.; Gärtner, F.; Jackstell, R.; Junge, H.; Dyson, P. J.; Laurenczy, G.; Ludwig, R.; Beller, M. Efficient dehydrogenation of formic acid using an iron catalyst. *Science* **2011**, *333*, 1733–1736.

(4) (a) Fukuzumi, S.; Kobayashi, T.; Suenobu, T. *ChemSusChem* **2008**, *1*, 827–834. (b) Himeda, Y.; Miyazawa, S.; Hirose, T. Interconversion between formic acid and H<sub>2</sub>/CO<sub>2</sub> using rhodium and ruthenium catalysts for CO<sub>2</sub> fixation and H<sub>2</sub> storage. *ChemSusChem* **2011**, *4*, 487–493.

(5) (a) Pan, Y.; Pan, C. L.; Zhang, Y.; Li, H.; Min, S.; Guo, X.; Zheng, B.; Chen, H.; Anders, A.; Lai, Z.; Zheng, J.; Huang, K.-W. Selective Hydrogen Generation from Formic Acid with Well-Defined Complexes of Ruthenium and Phosphorus - Nitrogen PN<sup>3</sup>-Pincer Ligand. *Chem. - Asian J.* **2016**, *11*, 1357–1360. (b) Filonenko, G. A.; van Putten, R.; Schulpen, E. N.; Hensen, E. J.; Pidko, E. A. Highly Efficient Reversible Hydrogenation of Carbon Dioxide to Formates Using a Ruthenium PNP-Pincer Catalyst. *ChemCatChem* **2014**, *6*, 1526–1530. (c) Czaun, M.; Goepfert, A.; Kothandaraman, J.; May, R. B.; Haiges, R.; Prakash, G. K. S.; Olah, G. A. Formic Acid As a Hydrogen Storage Medium: Ruthenium - Catalyzed Generation of Hydrogen from Formic Acid in Emulsions. *ACS Catal.* **2014**, *4*, 311–320. (d) Guerriero, A.; Bricout, H.; Sordakis, K.; Peruzzini, M.; Monflier, E.; Hapiot, F.; Laurenczy, G.; Gonsalvi, L. Hydrogen Production by Selective Dehydrogenation of HCOOH Catalyzed by Ru-Biaryl Sulfonated Phosphines in Aqueous Solution. *ACS Catal.* **2014**, *4*, 3002–3012. (e) Fukuzumi, S.; Kobayashi, T.; Suenobu, T. Unusually Large Tunneling Effect on Highly Efficient Generation of Hydrogen and Hydrogen Isotopes in pH-Selective Decomposition of Formic Acid Catalyzed by a Heterodinuclear Iridium–Ruthenium Complex in Water. *J. Am. Chem. Soc.* **2010**, *132*, 1496–1497. (f) Boddien, A.; Loges, B.; Junge, H.; Gärtner, F.; Noyes, J. R.; Beller, M. Continuous Hydrogen Generation from Formic Acid: Highly Active and Stable Ruthenium Catalysts. *Adv. Synth. Catal.* **2009**, *351*, 2517–2520. (g) Fellay, C.; Dyson, P. J.; Laurenczy, G. A Viable Hydrogen-Storage System Based On Selective Formic Acid Decomposition with a Ruthenium Catalyst. *Angew. Chem., Int. Ed.* **2008**, *47*, 3966–3968. (h) Loges, B.; Boddien, A.; Junge, H.; Beller, M. Controlled generation of hydrogen from formic acid amine adducts at room temperature and application in H<sub>2</sub>/O<sub>2</sub> fuel cells. *Angew. Chem., Int. Ed.* **2008**, *47*, 3962–3965.

- (6) (a) Celaje, J. J. A.; Lu, Z.; Kedzie, E. A.; Terrile, N. J.; Lo, J. N.; Williams, T. J. A prolific catalyst for dehydrogenation of neat formic acid. *Nat. Commun.* **2016**, *7*, 11308–11313. (b) Czaun, M.; Kothandaraman, J.; Goepfert, A.; Yang, B.; Greenberg, S.; May, R. B.; Olah, G. A.; Prakash, G. K. S. Iridium - Catalyzed Continuous Hydrogen Generation from Formic Acid and Its Subsequent Utilization in a Fuel Cell: Toward a Carbon Neutral Chemical Energy Storage. *ACS Catal.* **2016**, *6*, 7475–7484. (c) Matsunami, A.; Kayaki, Y.; Ikariya, T. Enhanced Hydrogen Generation from Formic Acid by Half-Sandwich Iridium(III) Complexes with Metal/NH Bifunctionality: A Pronounced Switch from Transfer Hydrogenation. *Chem. - Eur. J.* **2015**, *21*, 13513–13517. (d) Oldenhof, S.; Lutz, M.; de Bruin, B.; van der Vlugt, J. I.; Reek, J. N. H. Dehydrogenation of formic acid by Ir-bisMETAMORPhos complexes: experimental and computational insight into the role of a cooperative ligand. *Chem. Sci.* **2015**, *6*, 1027–1034. (e) Wang, Z.; Lu, S. M.; Li, J.; Wang, J.; Li, C. Unprecedentedly High Formic Acid Dehydrogenation Activity on an Iridium Complex with an N, N'-Diimine Ligand in Water. *Chem. - Eur. J.* **2015**, *21*, 12592–12595. (f) Manaka, Y.; Wang, W.-H.; Suna, Y.; Kambayashi, H.; Muckerman, J. T.; Fujita, E.; Himeda, Y. Efficient H<sub>2</sub> generation from formic acid using azole complexes in water. *Catal. Sci. Technol.* **2014**, *4*, 34–37. (g) Fujita, E.; Muckerman, J. T.; Himeda, Y. Interconversion of CO<sub>2</sub> and formic acid by bio-inspired Ir complexes with pendent bases. *Biochim. Biophys. Acta, Bioenerg.* **2013**, *1827*, 1031–1038. (h) Barnard, J. H.; Wang, C.; Berry, N. G.; Xiao, J. L. Long-range metal–ligand bifunctional catalysis: cyclometallated iridium catalysts for the mild and rapid dehydrogenation of formic acid. *Chem. Sci.* **2013**, *4*, 1234–1244. (i) Oldenhof, S.; de Bruin, B.; Lutz, M.; Siegler, M. A.; Patureau, F. W.; van der Vlugt, J. I.; Reek, J. N. H. Base-Free Production of H<sub>2</sub> by Dehydrogenation of Formic Acid Using An Iridium-bisMETAMORPhos Complex. *Chem. - Eur. J.* **2013**, *19*, 11507–11511. (j) Hull, J. F.; Himeda, Y.; Wang, W.-H.; Hashiguchi, B.; Periana, R.; Szalda, D. J.; James, T.; Muckerman, J. T.; Fujita, E. Reversible hydrogen storage using CO<sub>2</sub> and a proton-switchable iridium catalyst in aqueous media under mild temperatures and pressures. *Nat. Chem.* **2012**, *4*, 383–388. (k) Tanaka, R.; Yamashita, M.; Chung, L. W.; Morokuma, K.; Nozaki, K. Mechanistic studies on the reversible hydrogenation of carbon dioxide catalyzed by an Ir-PNP complex. *Organometallics* **2011**, *30*, 6742–6750.
- (7) (a) Sordakis, K.; Dalebrook, A. F.; Laurency, G. A Viable Hydrogen Storage and Release System Based on Cesium Formate and Bicarbonate Salts: Mechanistic Insights into the Hydrogen Release Step. *ChemCatChem* **2015**, *7*, 2332–2339. (b) Papp, G.; Csorba, J.; Laurency, G.; Joó, F. A Charge/Discharge Device for Chemical Hydrogen Storage and Generation. *Angew. Chem., Int. Ed.* **2011**, *50*, 10433–10435.
- (8) Bulushev, D. A.; Beloshapkin, S.; Ross, J. R. Hydrogen from formic acid decomposition over Pd and Au catalysts. *Catal. Today* **2010**, *154*, 7–12.
- (9) (a) Iguchi, M.; Himeda, Y.; Manaka, Y.; Matuoka, K.; Kawanami, H. Simple Continuous High-Pressure Hydrogen Production and Separation System from Formic Acid under Mild Temperatures. *ChemCatChem* **2016**, *8*, 886–890. (b) Iguchi, M.; Himeda, Y.; Manaka, Y.; Kawanami, H. Development of an Iridium-Based Catalyst for High-Pressure Evolution of Hydrogen from Formic Acid. *ChemSusChem* **2016**, *9*, 2749–2753.
- (10) Moret, S.; Dyson, P. J.; Laurency, G. Direct synthesis of formic acid from carbon dioxide by hydrogenation in acidic media. *Nat. Commun.* **2014**, *5*, 4017.
- (11) Onishi, N.; Ertem, M. Z.; Xu, S.; Tsurusaki, A.; Manaka, Y.; Muckerman, J. T.; Fujita, E.; Himeda, Y. Direction to practical production of hydrogen by formic acid dehydrogenation with Cp\* Ir complexes bearing imidazoline ligands. *Catal. Sci. Technol.* **2016**, *6*, 988–992.
- (12) (a) Ertem, M. Z.; Himeda, Y.; Fujita, E.; Muckerman, J. T. Interconversion of Formic Acid and Carbon Dioxide by Proton-Responsive, Half-Sandwich Cp\*Ir<sup>III</sup> Complexes: A Computational Mechanistic Investigation. *ACS Catal.* **2016**, *6*, 600–609. (b) Lu, Q. Q.; Yu, H. Z.; Fu, Y. Computational Study of Formic Acid Dehydrogenation Catalyzed by Al<sup>III</sup>-Bis(imino)pyridine. *Chem. - Eur. J.* **2016**, *22*, 4584–4591. (c) Li, J.; Li, J.; Zhang, D.; Liu, C. DFT Study on the Mechanism of Formic Acid Decomposition by a Well-Defined Bifunctional Cyclometalated Iridium(III) Catalyst: Self-Assisted Concerted Dehydrogenation via Long-Range Intermolecular Hydrogen Migration. *ACS Catal.* **2016**, *6*, 4746–4754. (d) Wang, W.-H.; Ertem, M. Z.; Xu, S.; Onishi, N.; Manaka, Y.; Suna, Y.; Kambayashi, H.; Muckerman, J. T.; Fujita, E.; Himeda, Y. Highly Robust Hydrogen Generation by Bioinspired Ir Complexes for Dehydrogenation of Formic Acid in Water: Experimental and Theoretical Mechanistic Investigations at Different pH. *ACS Catal.* **2015**, *5*, 5496–5504.
- (13) Wang, J. C.; Bauman, J. E., Jr. Complexes of 2, 2'-Bi-2-imidazoline with Transition Metal Ions. *Inorg. Chem.* **1965**, *4*, 1613–1615.
- (14) Frisch, M. J. T.; Trucks, G. W.; Schlegel, H. B.; Scuseria, G. E.; Robb, M. A.; Cheeseman, J. R.; Scalmani, G.; Barone, V.; Mennucci, B.; Petersson, G. A.; Nakatsuji, H.; Caricato, M.; Li, X.; Hratchian, H. P.; Izmaylov, A. F.; Bloino, J.; Zheng, G.; Sonnenberg, J. L.; Hada, M.; Ehara, M.; Toyota, K.; Fukuda, R.; Hasegawa, J.; Ishida, M.; Nakajima, T.; Honda, Y.; Kitao, O.; Nakai, H.; Vreven, T.; Montgomery, J. A., Jr.; Peralta, J. E.; Ogliaro, F.; Bearpark, M.; Heyd, J. J.; Brothers, E.; Kudin, K. N.; Staroverov, V. N.; Keith, T.; Kobayashi, R.; Normand, J.; Raghavachari, K.; Rendell, A.; Burant, J. C.; Iyengar, S. S.; Tomasi, J.; Cossi, M.; Rega, N.; Millam, J. M.; Klene, M.; Knox, J. E.; Cross, J. B.; Bakken, V.; Adamo, C.; Jaramillo, J.; Gomperts, R.; Stratmann, R. E.; Yazyev, O.; Austin, A. J.; Cammi, R.; Pomelli, C.; Ochterski, J. W.; Martin, R. L.; Morokuma, K.; Zakrzewski, V. G.; Voth, G. A.; Salvador, P.; Dannenberg, J. J.; Dapprich, S.; Daniels, A. D.; Farkas, O.; Foresman, J. B.; Ortiz, J. V.; Cioslowski, J.; Fox, D. J. GAUSSIAN 09 (Revision B.01); Gaussian, Inc.: Wallingford, CT, 2010.
- (15) (a) Kulkarni, A. D.; Truhlar, D. G. Performance of Density Functional Theory and Møller–Plesset Second-Order Perturbation Theory for Structural Parameters in Complexes of Ru. *J. Chem. Theory Comput.* **2011**, *7*, 2325–2332. (b) Zhao, Y.; Truhlar, D. G. Density functional theory for reaction energies: test of meta and hybrid meta functionals, range-separated functionals, and other high-performance functionals. *J. Chem. Theory Comput.* **2011**, *7*, 669–676. (c) Zhao, Y.; Truhlar, D. G. Benchmark Energetic Data in a Model System for Grubbs II Metathesis Catalysis and Their Use for the Development, Assessment, and Validation of Electronic Structure Methods. *J. Chem. Theory Comput.* **2009**, *5*, 324–333. (d) Valero, R.; Costa, R.; Moreira, I.; de, P. R.; Truhlar, D. G.; Illas, F. Performance of the M06 family of exchange-correlation functionals for predicting magnetic coupling in organic and inorganic molecules. *J. Chem. Phys.* **2008**, *128*, 114103. (e) Zhao, Y.; Truhlar, D. G. The M06 suite of density functionals for main group thermochemistry, thermochemical kinetics, noncovalent interactions, excited states, and transition elements: two new functionals and systematic testing of four M06-class functionals and 12 other functionals. *Theor. Chem. Acc.* **2008**, *120*, 215–241. (f) Zhao, Y.; Truhlar, D. G. Density Functionals with Broad Applicability in Chemistry. *Acc. Chem. Res.* **2008**, *41*, 157–167. (g) Zhao, Y.; Truhlar, D. G. Attractive noncovalent interactions in the mechanism of Grubbs second-generation Ru catalysts for olefin metathesis. *Org. Lett.* **2007**, *9*, 1967–1970. (h) Zhao, Y.; Schultz, N. E.; Truhlar, D. Exchange-correlation functional with broad accuracy for metallic and nonmetallic compounds, kinetics, and noncovalent interactions. *J. Chem. Phys.* **2005**, *123*, 161103.
- (16) Andrae, D.; Haeussermann, U.; Dolg, M.; Stoll, H.; Preuss, H. Energy-adjusted *ab initio* pseudopotentials for the second and third row transition elements. *Theor. Chim. Acta* **1990**, *77*, 123–141.
- (17) Marenich, A. V.; Cramer, C. J.; Truhlar, D. G. Universal Solvation Model Based on Solute Electron Density and on a Continuum Model of the Solvent Defined by the Bulk Dielectric Constant and Atomic Surface Tensions. *J. Phys. Chem. B* **2009**, *113*, 6378–6396.
- (18) Fukui, K. The path of chemical reactions - the IRC approach. *Acc. Chem. Res.* **1981**, *14*, 363–368.